

Thermal fluctuations, localization, and self-trapping in a polar crystal: Combined shell-model molecular dynamics and quantum chemical approach

Jacob L. Gavartin* and Alexander L. Shluger

Department of Physics and Astronomy, University College London, Gower Street, London WC1E 6BT, United Kingdom

(Received 7 February 2001; revised manuscript received 27 June 2001; published 10 December 2001)

We study the effects of thermal disorder on the electronic structure of crystalline MgO using a combination of shell model molecular dynamics (MD), semiempirical Hartree-Fock (HF), and *ab initio* plane-wave density-functional (DFT) calculations. Using the atomic configurations generated by MD, we calculate by the HF method the probability distributions for the on-site electrostatic potential and effective ionic charge, as well as electronic densities of states at the temperatures of 100, 300, and 500 K. We find the distribution for the on-site potential to be Gaussian, with a variance proportional to the temperature, while the ionic charge distribution is distinctly non-Gaussian. The potential and charge fluctuations contributing most to the electronic states in the valence-band tail are shown to have a structural pattern statistically similar to the one- and two-center small hole polarons. The HF calculations of the electronic excited states of thermally disordered MgO revealed a strong one-center localization of both electrons and holes at these sites. In contrast, DFT calculations of the same systems predicted a very weak localization or no localization of the exciton. We argue that both techniques lead to unsatisfactory conclusions in that the HF method *overestimates* the localization effect, and the DFT method *underestimates* it.

DOI: 10.1103/PhysRevB.64.245111

PACS number(s): 71.23.An, 71.35.-y, 72.15.Rn, 74.40.+k

I. INTRODUCTION

Exciton and polaron self-trapping through interaction with a polar medium has been attracting much attention over the last few decades (see Refs. 1 and 2 for recent reviews). Classical works by Rashba,² Toyozawa and co-workers,^{3,4} Sumi and Sumi,⁵ and others formulated general conditions for self-trapping to occur. Also the structure and spectroscopic properties of stable configurations of self-trapped excitons and polarons were studied both theoretically and experimentally in a wide range of materials.^{1,6} Time-resolved spectroscopy with femto-second resolution recently provided insights into the very early stages of self-trapping of electrons, holes, and excitons in alkali halides, alkaline-earth fluorides, oxides, chalcogenides, molecular crystals, and other systems.^{1,7-12} Nevertheless, the dynamics of the interaction of electrons and excitons with lattice vibrations, leading to the formation of self-trapped states, remains a formidable challenge for theory and experiment, and is mainly limited to general considerations.

In particular, Landau,¹³ and later Rashba² and Toyozawa,³ suggested the existence of a potential barrier between free and self-trapped polaron and exciton states in three dimensions, as schematically illustrated in Fig. 1. Assuming the existence of such a barrier, Sumi and Toyozawa⁴ suggested that the self-trapped species at the adiabatic minimum A_1 can be formed from the band states A_0 by tunneling through or thermal activation over the barrier B .

A number of authors proposed another mechanism in which atomic fluctuations due to thermal lattice disorder in the ground state lead to the formation of nucleation states responsible for self-trapping.^{4,5,14-16} In conjunction with this, a notion of a critical fluctuation was introduced, as the minimum lattice distortion required for self-trapping. The critical fluctuation is related to a position of the barrier point B in

Fig. 1. A slope of the potential surface reflects the forces acting upon the nuclei involved. In the electronic ground state these forces are restoring in nature, and drag the system toward a perfect lattice geometry and extended electronic states. However, due to the thermal phonon excitations, an electronic transition may occur from different points on the adiabatic surface of a ground state. Depending on the configuration coordinate Q , the electronic excitation may arrive on either side of the barrier on the adiabatic surface of the

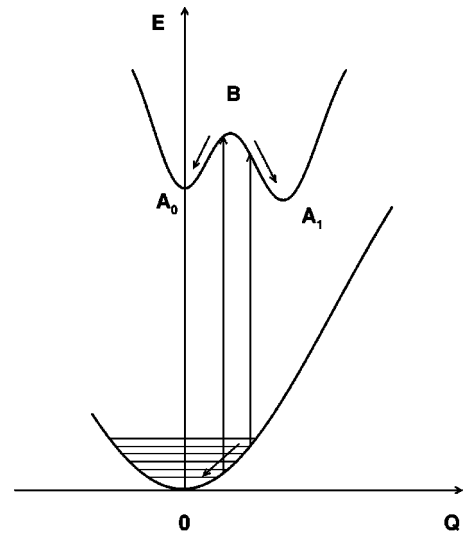


FIG. 1. A schematic diagram illustrating various adiabatic mechanisms for self-trapping. $Q=0$ corresponds to a perfect lattice geometry (and extended electronic states). The band excitation A_0 and the self-trapped state A_1 are separated by a barrier B . The self-trapping may occur either by tunneling through or a thermal activation over the barrier B , or by direct excitation into A_1 . The arrows in the ground and excited states indicate the direction of the force acting upon the atoms involved in the coordinate Q .

excited state. As a result, the excited state may subsequently evolve either toward a delocalized state A_0 or toward a localized state A_1 . Thus a necessary (but not sufficient) condition for self-trapping is the change of the direction of forces on atomic nuclei upon a sudden electronic excitation (Fig. 1).

Although generally accepted, this qualitative adiabatic picture proved to be difficult to quantify for specific systems. For example, the mechanism of transition between free and self-trapped polaron states has not yet been established, even in the most extensively studied case of alkali halides. Theoretical progress in this direction is important, especially in view of recent femtosecond pump-probe experiments in solids, which allow one to probe the dynamics of exciton relaxation. A particular example, which may also serve as an illustration of the motivation behind this work, concerns the early interpretation of pump-probe time-resolved optical spectroscopy of doped KI and RbI (Refs. 9 and 10) and NaBr, KBr, and RbBr.^{11,12} The observed transient optical absorption in these crystals was initially attributed to the formation of one-center hole polarons, and their subsequent transformation into the stable di-haloid V_k center form¹⁰ within less than 10 ps. Theoretical modeling based on static configurations supported this idea;^{10,17} however, the experimental evidence of the existence of transient one-center hole polaron states was shown to be inconclusive.¹⁸ Another example concerned recent self-consistent tight-binding molecular-dynamics calculations of polarons in TiO_2 .¹⁹ In this case, the average localization of electron polaron states induced by thermal disorder was demonstrated, but no atomistic models were deduced.

In order to study transient (or precursor) states for self-trapping, one can analyze the fluctuations of the potential experienced by the electrons. In particular, it is well established that, in ionic crystals, atomic disorder leads to a distribution of the on-site electrostatic potential. Kosłowski and co-workers demonstrated that in stoichiometric and metal-rich molten salts, the evolution of the electronic density of states (DOS) upon melting is intrinsically linked to the probability distribution for the on-site electrostatic potential.^{20–22} Using a tight-binding approach, they found that the probability distribution of the on-site electrostatic potential induced by the topological disorder is generally Gaussian, in agreement with predictions of linear graphical theories for simple liquids.²³ The width of the distribution in the melt is found to be of the order of 1 eV, which in turn results in the appearance of tails in the electronic DOS.

Similar questions regarding the scale of fluctuations of the on-site electrostatic potential induced by just *thermal* atomic disorder in an otherwise perfect crystal have not yet been addressed. In this paper we consider whether any of the thermal lattice fluctuations are capable of trapping electrons and/or holes produced by the optical excitation, and what the atomic structure of such fluctuations is. We focus mainly on developing a methodology for analyzing thermal fluctuations in the ionic crystals and their correlation with the electronic structure of the ground and lowest excited states.

To demonstrate our approach, we consider a crystalline

magnesium oxide. At ambient pressure and temperature MgO possesses a rock-salt-type structure quite common for binary wide-gap dielectrics. This makes MgO a good generic system for discussing general issues of localization and thermal fluctuations in these materials.

To model the atomistic and electronic properties associated with thermal disorder, we consider probability distributions of the on-site electrostatic potential and fluctuations of the ionic charge at different temperatures, and analyze their effect on electron band tails and charge localization. This allows us to pinpoint specific atomic displacements coupled to these fluctuations. We then calculate the electronic excited states, and analyze the charge- and spin-density distributions and their interrelation with potential fluctuations in the ground state. Part of this work was briefly reported elsewhere.^{24,25}

Our approach to an analysis of the effect of disorder on the electronic structure is in many ways similar to that used recently in the studies of the electronic structure of amorphous silicon,²⁶ silicon dioxide,^{27,28} molten salts,^{20,21} and charge-transfer alloys.²² Two alternative techniques have been applied in these calculations. One is to undertake a molecular-dynamics simulation within density functional theory²⁷ (DFT), where the charge density self-consistently follows the classical evolution of nuclei. A number of instantaneous atomic configurations is then selected for the analysis of the electronic structure. Another approach is to generate atomic configurations within classical molecular dynamics using empirical interatomic potentials, and then to calculate their electronic structure.^{26,28}

The former approach is more consistent, since both the nuclear dynamics and the electronic properties are considered within the same Hamiltonian. However, it cannot treat large systems, and the local approximation for the exchange interaction widely used in DFT schemes may lead to uncontrolled errors in predicting the character of charge localization.^{25,29–32} A correlation analysis between atomic fluctuations and electronic structure requires a representative number of at least short- and medium-range fluctuations. Therefore, we opted for the second approach, allowing for a treatment of larger systems. However, the use of two Hamiltonians containing different approximations may also lead to inconsistencies. Since similar approaches are used in other studies, we present an analysis of this problem.

The main result of this paper concerns the prediction that the characteristic atomic fluctuations coupled to the electron states deep in the valence-band tail have a structural pattern statistically similar to the one- and two-center small hole polarons characteristic of dielectrics with a rock-salt structure. Furthermore, the corresponding local charge fluctuations are also qualitatively similar to those of polarons in the initial stage of self-trapping. In order to demonstrate that such fluctuations indeed serve as precursors for exciton self-trapping, we carry out semiempirical Hartree-Fock and plane-wave density-functional calculations of excited states in thermally disordered crystals.

The paper is organized as follows. In Sec. II we describe the modeling procedure. Section III is concerned with a correspondence between the results obtained within shell model

and Hartree-Fock calculations. The properties of the electronic densities of states are discussed in Sec. IV. In Sec. V we establish a correlation between the on-site potential and charge fluctuations and local atomic arrangements in the MgO crystal. The calculations of the lowest electronic excitations are presented in Sec. VI, while a discussion and conclusions are given in Sec. VII.

II. MODELING PROCEDURE

The calculation of thermodynamic properties of a particular disordered system involves a statistical averaging of the expectation value of the relevant quantum-mechanical operator with the system's potential distribution function. In this case a detailed origin of this distribution is unimportant. However, a study of microscopic effects requires detailed information concerning the correlation between fluctuations in the atomic displacements, electron potential, and electronic states. Since the potential distribution function, at least in principle, can be recovered from the system's dynamics, both the thermodynamic characterization of disorder and the microscopic correlations can be studied within the same framework of molecular-dynamics simulations.

To characterize thermal disorder, we employ a relatively simple yet reliable shell model molecular-dynamics (MD) approach. We then use representative instantaneous atomic configurations to evaluate the electronic structure within a semiempirical Hartree-Fock method, and thus implicitly employ the Born-Oppenheimer approximation.

Exciton self-trapping is often associated with electron coupling to lattice optical phonons. Therefore, it is essential that the models employed adequately describe the frequency-dependent dielectric response of a system studied.³³⁻³⁵ We use the microcanonical MD (constant energy, volume and number of particles) approach implemented in the GULP code,³⁶ where the electronic polarization is treated within the shell model. In this approach the massless shells are statically relaxed to their equilibrium positions at each atomic time step. We employ the interatomic shell model potentials due to Stoneham and Sangster.³⁷ In this model the ions interact electrostatically and elastically via the pairwise central potentials of Buckingham form. The ionic charges are taken to be $\pm 2e$ for Mg and O respectively, and cations are considered unpolarizable. The parameters for the short-range interaction are fitted to reproduce the experimental lattice geometry and the dielectric and elastic constants. This set of potentials was extensively tested for MD modeling by Fincham *et al.*³⁴ and was found to describe fairly well the phonon dispersion, the dielectric and elastic constants at ambient pressure and temperature, and the volume thermal expansion and compressibility of crystalline MgO.

We consider the MD of a cubic supercell of 512 ions (a $4 \times 4 \times 4$ extension of the crystalline unit cell of four molecules) subject to periodic boundary conditions, at three temperatures: 100, 300, and 500 K. In all calculations, a time step of 0.5 fs assures that the required accuracy in shell relaxation is achieved on average within 13 iterations of the variable metric BFGS algorithm.³⁸ After equilibration at each temperature, a production MD run for 10 ps was performed.

To analyze the influence of thermal disorder on the electronic structure, an ensemble averaging of the electronic properties is required. We generate sets of atomic configurations by drawing them randomly from the instantaneous configurations generated by MD simulations. The MD frames were sufficiently separated in time so that they can be considered uncorrelated. In the microcanonical ensemble, an electron DOS can be averaged with the potential-energy probability distribution. Assuming the latter to be Gaussian, an average electron density of states is given by the expression

$$\langle \mathcal{D}(\varepsilon) \rangle = \frac{1}{\mathcal{M}\sigma\sqrt{\pi}} \sum_i^{\mathcal{M}} e^{-\langle E \rangle - E_i)^2 / 2\sigma^2} \mathcal{D}(\varepsilon), \quad (1)$$

where $\langle E \rangle$ and σ^2 are respectively the mean potential energy and its mean square deviation calculated from the MD run, and E_i and $\mathcal{D}(\varepsilon)$ are the potential energy and DOS of the i th instantaneous configuration. The average is taken independently for each point on the electronic energy grid ε over the \mathcal{M} sets of atomic configurations. We note that the width of the potential-energy distribution σ depends on a number of particles as $\approx 1/\sqrt{N}$. Thus the configurations drawn from the tails of the potential-energy distribution of a finite system somewhat overestimate the density of high-amplitude fluctuations. Alternatively, assuming that the system modeled is sufficiently large, one can average only over configurations with energies close to the distribution's maximum, i.e., those with $E_i \approx \langle E \rangle$. This approach would generally underestimate the characteristic amplitudes of the short-range fluctuations. We examined both approaches, and found that for thermal disorder below 600 K, the electron DOS averaged over the sets drawn by these two methods are indistinguishable within our statistical accuracy. We resolved on the second approach, as it uses the information on the mean value of the potential energy, and, for sufficiently large systems, is independent of the system's size.

To calculate electronic structure of chosen atomic configurations we use a supercell approach and the semiempirical linear combination of atomic orbitals (LCAO) Hartree-Fock method in the intermediate neglect of differential overlap (INDO) approximation, implemented in the SYM-SYM package.³⁹ The INDO parameters were fitted to represent the geometry of the MgO molecules, the lattice constant, the valence band, and the energy gap widths of the perfect MgO crystal.⁴⁰ In the LCAO approach single particle eigenfunctions $\psi_\varepsilon(\mathbf{r})$ are expressed as linear combinations of atomic orbitals (AO's). In the case of MgO, we consider s -type AO's on magnesium and s - and p -type AO's on oxygen ions,

$$\psi_\varepsilon(\mathbf{r}) = \sum_{i\alpha} c_{i\alpha}(\varepsilon) \phi_{i\alpha}(\mathbf{r} - \mathbf{r}_i), \quad (2)$$

where i enumerates the atoms and α the atomic orbitals centered in \mathbf{r}_i ; $c_{i\alpha}(\varepsilon)$ are the normalized components of the eigenvector belonging to the eigenvalue ε .

The degree of localization of the single-particle eigenstates, $\psi_\varepsilon(\mathbf{r})$, was studied by means of the inverse participation function $p(\varepsilon)$ (Ref. 41):

$$p^{-1}(\varepsilon) = \sum_{i\alpha} c_{i\alpha}^4(\varepsilon). \quad (3)$$

The inverse participation function gives an indication of how many atoms the state in question is spread over. In the limit of truly extended states, $\psi_\varepsilon(\mathbf{r})$ is uniformly spread over the sublattice (in MgO, valence-band states are localized mainly on anions, while the conduction band states reside on cations). Thus the coefficients $c_i^2 = \sum_\alpha c_{i\alpha}^2$ are approximately independent of i and, due to the normalization of the eigenstates, $c_i^2 \approx \text{const}(i) = 1/N_s$, where N_s is the number of atoms in the sublattice. Therefore, for extended states, $p(\varepsilon) \approx N_s$. In the opposite limit of complete one-site localization ($c_i^2 = \delta_{ij}$), $p(\varepsilon) \approx 1$.

In addition to the one-electron spectrum and $p(\varepsilon)$, we also calculate effective ionic charges $\{q_i\}$ (using the modified Löwdin population analysis⁴²) and on-site electrostatic potentials $\{U_i\}$ resulting from the charge distributions. These data are used to generate the probability distributions of the electrostatic potential and the ionic charges. In order to study correlations between the localization of electronic states and fluctuations of the ionic charge and on-site electrostatic potential, we introduce the energy-dependent electrostatic potential fluctuation function $\Delta\mathcal{U}(\varepsilon)$,

$$\Delta\mathcal{U}(\varepsilon) = \sum_{i\alpha} c_{i\alpha}^2(\varepsilon)(U_i - \bar{U}), \quad (4)$$

and the energy-dependent ionic charge fluctuation function $\Delta\mathcal{Q}(\varepsilon)$,

$$\Delta\mathcal{Q}(\varepsilon) = \sum_{i\alpha} c_{i\alpha}^2(\varepsilon)(q_i - \bar{Q}), \quad (5)$$

where U_i and q_i are the electrostatic potential and the ionic charge on the atom i , respectively, and \bar{U} and \bar{Q} are the corresponding distribution averages. The correlation functions $\Delta\mathcal{U}(\varepsilon)$ and $\Delta\mathcal{Q}(\varepsilon)$ exploit an idea similar to the one behind the inverse participation function: they significantly deviate from zero only for the states where both the localization (substantial $c_{i\alpha}^2$) and the potential (or charge) fluctuation of the particular sign occur on the same ions.

III. TWO HAMILTONIANS

Since the two (shell model and INDO Hartree-Fock) Hamiltonians involve different approximations and generally represent systems with different vibrational properties, the predicted thermodynamic properties will also differ. Therefore, the generation of an ensemble of atomic configurations within one Hamiltonian and the subsequent analysis of the properties of this ensemble within another Hamiltonian requires justification.

First, we note that the (NVE) MD generates the microcanonical ensemble ($E_{tot} = \text{const}$). Thus, at each atomic configuration, the fluctuations of the system's potential and kinetic energy strictly anticorrelate, so the probability distributions of the potential and kinetic energies are identical. Therefore, the potential-energy distribution uniquely

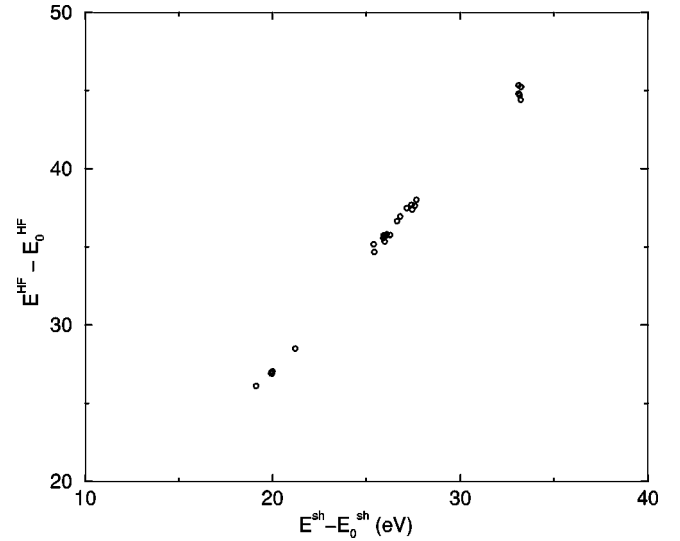


FIG. 2. The energy, less the energy of the perfect crystal, calculated within the shell model approach plotted against the energy obtained within the INDO HF approach for the same set of atomic configurations.

characterizes a microcanonical ensemble at a given temperature. Second, being unable to produce sufficiently large and long MD simulations within the Hartree-Fock (HF) method, we cannot test whether the classical and HF models generate similar potential-energy distributions. Instead, we compare potential-energy distributions obtained with two Hamiltonians using the same ensemble of configurations. To achieve this, we compare the potential energies calculated in the static shell model and in the INDO HF methods for atomic configurations generated by the shell model MD at $T=300$ and 500 K, and by an uncorrelated Gaussian atomic disorder model with given mean-square atomic displacements. The potential energies obtained within the shell model and HF calculations are plotted one against the other in Fig. 2. First we note a good linear correlation between the energies in the two approaches. A small systematic energy difference (a non-unit gradient of the nearly linear curve) is of the order of 0.05 eV per MgO molecule. This is largely attributed to the difference in the description of the electrostatic interaction as discussed below. The linear correlation between the energies means that the configurations, close in energy in one approach, also have similar energies in another. In particular, we have calculated the HF energies of several atomic configurations, whose energies are almost degenerate within the shell model approach. The scatter of the corresponding HF energies of the configurations at $T=500$ K did not exceed 1 eV (Fig. 2).

The next quantity of interest, which can also be evaluated within both approaches, is the probability distribution for the on-site electrostatic potential,

$$g_s(U) = \langle \delta(U_i - U) \rangle_{i \in s}, \quad (6)$$

where

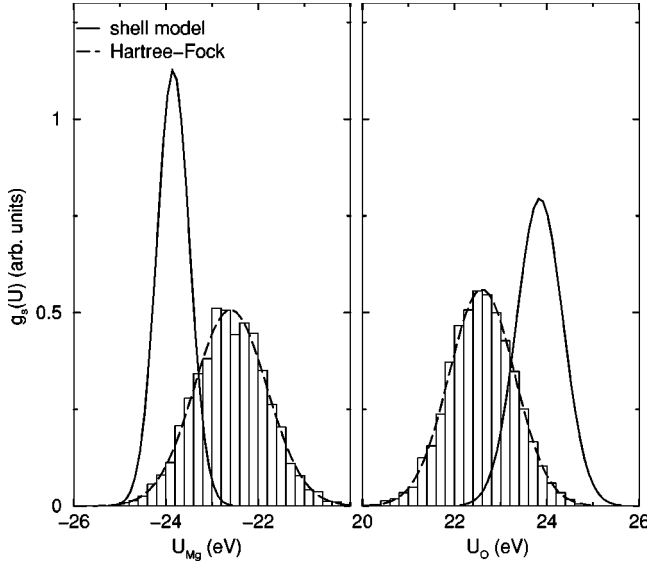


FIG. 3. The Gaussian approximation of the on-site electrostatic potential probability distributions for the magnesium (left) and oxygen (right) sublattices calculated at $T=500$ K within the shell model (solid line) and within the INDO HF approach (dashed line). The histograms of the raw data for the INDO HF model are also shown for a comparison.

$$U_i = \sum_{j(\neq i)} \frac{q_j}{|\mathbf{r}_i - \mathbf{r}_j|}. \quad (7)$$

Here $\delta(x-x_0)$ is the Dirac δ function; q_j and \mathbf{r}_j denote the charge and the position vector of the atom j , respectively; j runs over all the atoms in the system; s denotes the sublattice ($s=\text{Mg}$ or O); and the angular brackets indicate an ensemble average over the atomic sites belonging to the sublattice s . In the shell model, the sum is taken over all the cores and shells in the system.

The probability distributions $g_{\text{Mg}}(U)$ and $g_{\text{O}}(U)$ evaluated within the shell model and INDO HF methods are depicted in Fig. 3. In both cases the probability distributions were evaluated using the same set of six different ionic configurations of 512 atoms, generated by the shell model MD at $T=500$ K. We have found distributions predicted by both methods to be Gaussian within the statistical accuracy of our calculations. Therefore we plot $g_s(U)$ using Gaussian functions with the mean value \bar{U}_s and variance σ_s^2 of the raw data. The actual distribution histograms obtained by the INDO HF approach are also shown for comparison. We note that the mean values \bar{U}_s and variances σ_s^2 of both distributions differ significantly (Fig. 3). The HF mean value is smaller (in absolute value), but the variance is larger than the corresponding values in the shell model (SM) for both sublattices, that is $|\bar{U}_s^{\text{HF}}| < |\bar{U}_s^{\text{SM}}|$, and $(\sigma_s^{\text{HF}})^2 > (\sigma_s^{\text{SM}})^2$, ($s=\text{Mg}$ or O).

These discrepancies can be rationalized recalling that the distribution $g_s(U)$, as defined in Eq. (6), depends upon the ionicity of the system via the ionic charges q_j . These charges are constant within the shell model approach [the total (core plus shell) ionic charges for Mg and O are equal

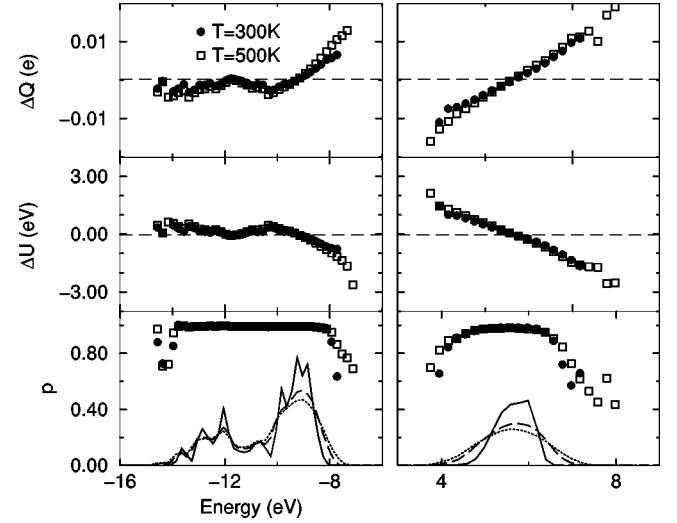


FIG. 4. The electron densities of states, the participation function (bottom), the energy-dependent potential fluctuation (middle), and the energy-dependent charge fluctuation (top), shown for the top valence and conduction bands (left and right panels, respectively). All functions are products of averaging over six atomic configurations at temperatures 300 K (circles and dashed line) and 500 K (squares and dotted line). The electron densities of states are obtained by a Gaussian broadening (0.2 eV), are the same for all temperatures. The solid line corresponds to the DOS of the perfect MgO crystal.

to $q = \pm 2e$ in the present model³⁷). On the other hand, the effective charges obtained in the quantum-chemical calculations for the perfect MgO lattice are lower: $\pm 1.82e$. Consequently, the mean on-site electrostatic potential predicted by the HF calculations is smaller. We note that the mean electrostatic potentials \bar{U}_s^{HF} and \bar{U}_s^{SM} are equal to the respective values of the on-site Madelung potential in the perfect lattice. As we discuss below, this may not be a general feature, but at this point it verifies our argument about the origins of the difference in the distributions.

The difference between the variances of the distributions can also be explained by noting that the fluctuations of the electrostatic potential are coupled to the fluctuations of the effective ionic charges q_j . This effect is neglected within the shell model, but is accounted for within the quantum-chemical approach. Thus the distribution $g_s(U)$, in Eq. (6), is affected by the fluctuations of ionic charges q_j as well as by the fluctuations in atomic positions, so that the variance σ_s^2 obtained in the HF method is larger. In the rest of this paper we shall concentrate on the probability distributions obtained within quantum-chemical calculations of the configurations generated by the shell model MD.

IV. ELECTRON DENSITY OF STATES

The electron DOS averaged over the atomic configurations generated at 300 and 500 K, and that for the perfect MgO lattice, are shown in the lower panel of Fig. 4. The density of states is constructed from the one-electron spectrum calculated within the Hartree-Fock method at the Γ

point of the supercell of 512 atoms. The calculated one-electron energies are broadened by Gaussians with the dispersion parameter equal to 0.2 eV, the same for all temperatures. The DOS is averaged over sets of 6–16 atomic configurations at each temperature. We note that the variations in DOS calculated for different geometries at given temperatures are small. In this sense the DOS calculated for a single disordered configuration of 512 atoms serves as a good approximation of the ensemble average. The HF calculations predict the valence-band (VB) states to originate almost exclusively from p -type atomic orbitals of oxygen ions, while the conduction-band (CB) states originate from the s orbitals of the magnesium ions.

The tails in the DOS induced by thermal fluctuations are evident in both valence and conduction bands. The absence of band tails at the lower energy end of VB's is due to a small number of states. As can be seen in Fig. 4, our calculations predict a valence-band-tail expansion of ≈ 1 eV, as the temperature increases from 0 to 500 K.

Next we discuss the relation between charge and on-site electrostatic potential fluctuations and the localization of electronic states in the DOS tails. In the lower panel of Fig. 4 we depict the average participation function [Eq. (3)] for the one-electron states contributing to the valence and conduction bands of a MgO crystal calculated at 300 and 500 K. The participation function $p(\varepsilon)$ is normalized to the number of particles in the system. The middle and top panels in Fig. 4 show, respectively, the average energy-dependent electrostatic potential and charge fluctuation functions, as defined by Eqs. (4) and (5). The averaging for all quantities was performed over energy intervals of 0.2 eV and over sets of six atomic configurations for each temperature. A decrease of the participation function in the tail regions indicates a weak localization of the electronic states. This localization is coupled to the electrostatic potential fluctuations $\Delta U < 0$ for the valence-band tail and $\Delta U > 0$ for the conduction-band tail. As noted above, the valence-band states originate predominantly from oxygen p -type atomic orbitals, and the electrostatic potential on oxygen sites \bar{U}_O is positive (see Fig. 3). Therefore, it is not surprising that states in the high-energy VB tail are induced by the potential fluctuations in the oxygen sublattice, such that $u_O < \bar{U}_O$. Similarly, the potential fluctuations reducing the negative potential on a magnesium site are responsible for the states in the lower tail of the conduction band. In further discussion we shall refer to such fluctuations as *relevant*, to distinguish them from all other fluctuations not responsible for the states in the VB and CB tails of the electron DOS.

The energy-dependent charge fluctuations ΔQ (see the top panel of Fig. 4) strongly correlate with the potential fluctuations. This reflects the fact that the fluctuating sites, on which the localization occurs, experience small but systematic charge fluctuations. The oxygen atoms, on which the VB tail states are mainly localized, are less negative, and the magnesium atoms, on which the CB tail states are localized, are less positive than the respective mean ionic charges.

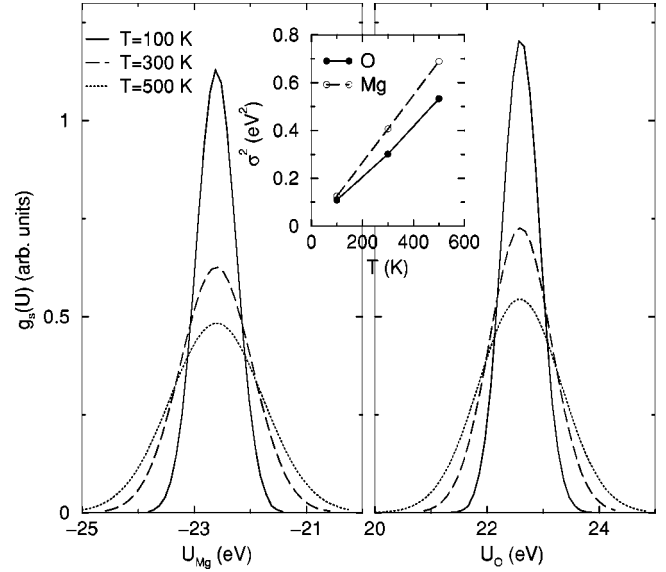


FIG. 5. The on-site electrostatic potential distributions for the magnesium (left) and oxygen (right) sublattices calculated within the INDO HF approach at 100, 300, and 500 K (solid, dashed, and dotted lines respectively). The inset shows the temperature dependence for variances of the potential distributions.

V. PROBABILITY DISTRIBUTIONS FOR THE ON-SITE ELECTROSTATIC POTENTIAL AND IONIC CHARGE

The calculated on-site electrostatic potential distribution for the cation and anion sublattices at 100, 300, and 500 K are shown in the left and right panels of Fig. 5, respectively. As mentioned above, the distributions are Gaussian, with mean values \bar{U}_s , independent of the temperature and equal to the respective Madelung potentials in the perfect lattice. The variances of the potential distributions, shown in the inset of Fig. 5 are, as expected, proportional to the temperature. It is remarkable that the dispersion of the distributions generated by thermal disorder at comparatively low temperatures are of the order of 0.5–0.8 eV, which results in the substantial tails in the electron DOS (Fig. 4). We observe that the variance of the potential distribution is smaller for the oxygen sublattice than for the magnesium sublattice. At the same time, mean-square ionic displacements (MSD's) demonstrate the opposite trend, i.e., they are larger for the oxygen sublattice (an atomic mass of oxygen is about 1.5 times smaller than that of magnesium).

The temperature dependence of the shape of the potential distribution can be rationalized by considering two extreme qualitative models for atomic dynamics: an oscillating atom in an effective potential well as in the Einstein model,⁴³ and an atom in an oscillating well model. The probability distributions of the on-site electrostatic potential in the two models are distinctly different, as illustrated schematically in Fig. 6. In the case of an *oscillating atom*, the on-site electrostatic potential cannot exceed its value at the corresponding perfect lattice site U_0 . Therefore, the resulting potential probability distribution for the *oscillating atom* will be asymmetric with the maximum shifted from U_0 toward lower amplitudes.

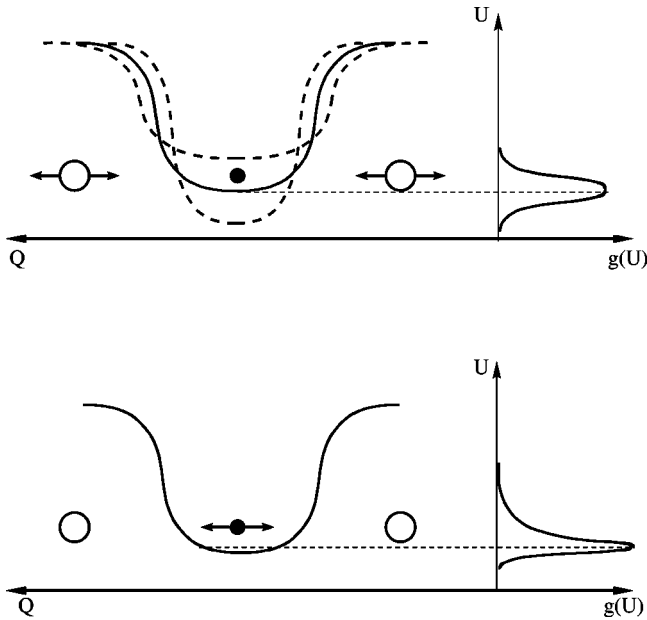


FIG. 6. A schematic diagram illustrating the on-site potential fluctuations and their probability distributions in the *oscillating-well* (top) and *oscillating-atom* (bottom) models.

Conversely, the *oscillating well* model will result in a Gaussian-shaped distribution centered near the U_0 , providing the oscillations are nearly harmonic.

In the case of a rock-salt-structured polar dielectric, the on-site potential is dominated by the Madelung potential, which is flat to the second order with respect to ionic displacements from the lattice site in all crystallographic directions. At the same time, the on-site electrostatic potential depends hyperbolically on the breathing displacement of the nearest ions. Thus it is conceivable that the shape of the potential distribution in the rock-salt-structured crystals will correspond more to that in the *oscillating well* model. This agrees with our calculations for a MgO crystal. One may further suggest that the highest on-site potential fluctuations, contributing to the tails in the potential distribution, originate mainly from the breathing inward and outward displacements of the nearest neighbors. This would explain the difference in the variances of the potential distributions on anion and cation sublattices (see Fig. 5)—larger MSD's in the oxygen sublattice result in larger fluctuations (and, hence, larger variances) of the on-site electrostatic potential on a magnesium site.

As mentioned above, the on-site potential fluctuations are coupled to ionic charge fluctuations, giving a finite width to the ionic charge distributions. The charge distributions for the oxygen and magnesium ions in MgO, calculated using a Löwdin population analysis for temperatures of 100, 300, and 500 K, are shown in Fig. 7. Unlike the electrostatic potential probability distributions, the charge probability distributions are distinctly asymmetric with the asymmetry increasing with thermal disorder (temperature). Clearly, for small on-site potential fluctuations the amplitude of the corresponding charge fluctuation is defined by the local chemical potential. Therefore, one would expect the charge distri-

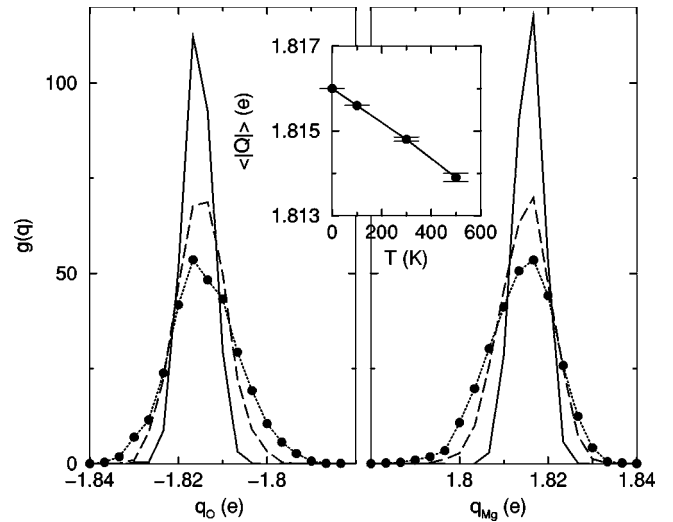


FIG. 7. Charge probability distribution functions for oxygen (left) and magnesium (right) sublattices calculated at 100, 300, and 500 K (solid, dashed, and dotted lines, respectively). The inset shows the temperature dependence of a mean ionic charge. The $T = 0$ K value corresponds to the ionic charge in a perfect MgO lattice.

butions to be symmetrical around their maxima. For stronger fluctuations, however, the difference between the in-crystal ionization energies and the ionic electron affinities becomes larger. Hence the oxygen charge distribution has a longer positive tail, while the magnesium distribution has a longer negative tail (Fig. 7). The temperature enhancement of the asymmetry in charge distributions also causes a small shift in their mean values \bar{Q}_s with respect to the distribution's maxima. Thus an effective ionicity of a crystal generally decreases with temperature, as shown in the inset of Fig. 7. This effect is small for MgO, but may become larger for less rigid ionic compounds.

The on-site electrostatic potential and ionic charge are coupled due to the self-consistency of the charge density and the potential distribution it generates. Therefore, the charge and potential fluctuations are correlated, and fluctuations of the on-site electrostatic potential have corresponding fluctuations of the ionic charge. This correlation is clearly seen in Fig. 4. The fact that these fluctuations also correlate with the states in the band tails opens possibilities for further analysis. In particular, in order to establish a relation between the states in the DOS with characteristic atomic fluctuations, one can consider correlations with either charge or potential fluctuations. We analyze the correlation of atomic displacements with *charge* fluctuations, since the charge conservation argument can then be employed for physical clarity.

VI. ANALYSIS OF CHARGE FLUCTUATIONS

Any ionic charge fluctuation can be viewed as a deviation from local lattice charge neutrality. Due to the global charge neutrality, this deviation must be exactly compensated for at any instant by the opposite charge fluctuations elsewhere in the lattice. This gives rise to spatial correlations between the

TABLE I. The charge correlation function as defined by Eq. (8), calculated at different temperatures. The statistical error bars are shown in brackets.

T (K)	100 K	300 K	500 K
$\gamma_{OMg}(001)$	0.15 (0.03)	0.15 (0.03)	0.15 (0.01)
$\gamma_{MgMg}(110)$	0.03 (0.02)	0.04 (0.02)	0.03 (0.01)
$\gamma_{OO}(110)$	0.01 (0.02)	0.03 (0.01)	0.04 (0.01)
$\gamma_{MgMg}(200)$	-0.14 (0.04)	-0.16 (0.03)	-0.15 (0.04)
$\gamma_{OO}(200)$	-0.05 (0.04)	-0.06 (0.02)	-0.10 (0.04)

ionic charge fluctuations. The mirror symmetry of the charge distributions on the magnesium and oxygen sublattices seen in Fig. 7, suggests that the charge compensation in MgO should occur predominantly in the opposite sublattice. In order to test this conjecture, we introduce a charge correlation function at the coordination sphere z_s ,

$$\gamma_{ss'}(z_s) = \frac{1}{\sigma_s \sigma_{s'}} \sum_{i \in s, i' \in s'} (q_i - \bar{Q}_s)(q_{i'} - \bar{Q}_{s'}) \times \theta(r_{ii'} - r_{1z}) \theta(r_{2z} - r_{ii'}), \quad (8)$$

where i and i' run over all the atoms of the sublattices s and s' respectively, σ_s is a root-mean-square deviation of the charge probability distribution on the sublattice s (thus, $\gamma_{ss}(0) = 1$). The product of the Heaviside step functions $\theta(x - r_{1z}) \theta(r_{2z} - x)$ insures that the averaging is taken over the spherical shells containing all the atoms from a given coordination sphere [i.e., for the first coordination sphere, we chose $r_{11} = a_0/2$, and $r_{21} = a_0(1 + \sqrt{2})/2$, where a_0 is the nearest Mg-O distance in the perfect lattice, etc.]. In the case of charge compensation at a coordination sphere z_s , the charge correlation function, $\gamma_{ss'}(z_s)$ would assume a negative number.

The values of charge correlation functions calculated for up to the third-nearest neighbors are summarized in Table I. It is seen that $\gamma_{OMg}(100)$ (nearest neighbor O-Mg pairs) is significantly positive, that is, on average the fluctuations on the oxygen and on the nearest-neighbor magnesium atoms are of the same sign. Thus the charge compensation, as introduced above, does not generally occur on the nearest neighbors.

Next we observe that the cation-cation charge correlation is stronger than that of the anion-anion correlation, and that the values of $\gamma_{ss}(110)$ (closest O-O or Mg-Mg pairs) fluctuations are also significantly positive, indicating the tendency for the same sign fluctuations to occur on the (110) pairs. Finally, the $\gamma_{OO}(200)$ and $\gamma_{MgMg}(200)$ are found to be negative and, for the cation-cation case, comparable in amplitude with the $\gamma_{OMg}(100)$. Therefore, a significant part of the charge-compensating fluctuations occurs on the second-nearest (200) neighbors of the same sublattice, contrary to our initial assumption. We note that the charge correlations between more distant atoms are significantly smaller; therefore, we do not consider them here.

The strong anticorrelation between the next-nearest-neighbor ions of the same sort [(200) pairs] can be rational-

ized within the *oscillating well* model introduced earlier. Indeed, the potential (and charge) fluctuations on an ion are primarily determined by the “breathing” component of the displacement of its oppositely charged nearest neighbors. Let us consider an O-Mg-O sequence of ions along the (100) crystalline axis. The Mg ion participating in the “breathing in” phase for the left oxygen contributes to the “breathing out” phase for the right oxygen, thus triggering the opposite sign fluctuations on them. In other words, the anticorrelation between the (200) ions is mediated by a (100) ion of another type between them. In agreement with this picture, the charge correlation $\gamma_{MgMg}(200)$ is stronger than $\gamma_{OO}(200)$ due to the larger MSD’s of less massive oxygen ions (cf. Table I).

As seen in Table I, the calculated charge correlation functions do not display dramatic temperature dependence. This can be related to the high frequency (and, therefore, low thermal population) of the relevant phonons. Our shell model calculations for the Γ -point LO phonon predict values of $\omega_{LO}(000) = 732 \text{ cm}^{-1}$ and $\omega_{TO}(1/2, 1/2, 0) = 451 \text{ cm}^{-1}$ for the TO (110) phonon.

The above interpretation of the charge correlation implies that specific fluctuations of the ionic charge are coupled to some particular short- or medium-range instantaneous atomic arrangements. To determine the statistical importance of this coupling, let us consider the *relevant* charge fluctuations on oxygen ions. We define the fluctuation to be *relevant*, when an oxygen charge is more positive than the average by more than a certain threshold value Q^{th} ,

$$q_i - \bar{Q}_O > Q^{th} = \alpha^q \sigma_O, \quad (9)$$

where α^q is an arbitrary dimensionless charge fluctuation threshold parameter, measured by root-mean-square deviations σ_O of the charge probability distribution, $g_O(q)$, for the oxygen sublattice (Fig. 7). As established in Sec. V, atoms experiencing such fluctuations contribute most to the states in the VB tail (Fig. 4). Similarly, *relevant* fluctuations on Mg atoms, contributing most into the conduction-band tail, are defined such that $q_i - \bar{Q}_{Mg} < -\alpha^q \sigma_{Mg}$.

To establish a structural pattern around the fluctuating sites, let us compare the partial radial distribution function (RDF) “as seen” from the fluctuating oxygen and magnesium atoms, and the total RDF averaged over all the atoms (Fig. 8). Even for a relatively small fluctuation threshold ($\alpha^q = 1.8$), a clear pattern of atomic configurations emerges: for atoms experiencing *relevant* charge fluctuations, the first RDF peak is shifted toward larger distances. This reflects predominantly outward “breathing” displacements of the atoms around the fluctuating sites shown in the insets of Fig. 8. We also note a marginal shift of the second RDF peak toward smaller distances for both oxygen and magnesium atoms. Further analysis demonstrates that this latter shift originates from the contribution from the *(110) pairs of fluctuating atoms* (that is, nearest-neighbor anion-anion or cation-cation pairs). The interatomic distance in such pairs is on average slightly smaller than the crystal average value of $a_0\sqrt{2}$ as illustrated in Fig. 9. Furthermore, we find that the (110) pairing of the on-site fluctuations is statistically significant. To

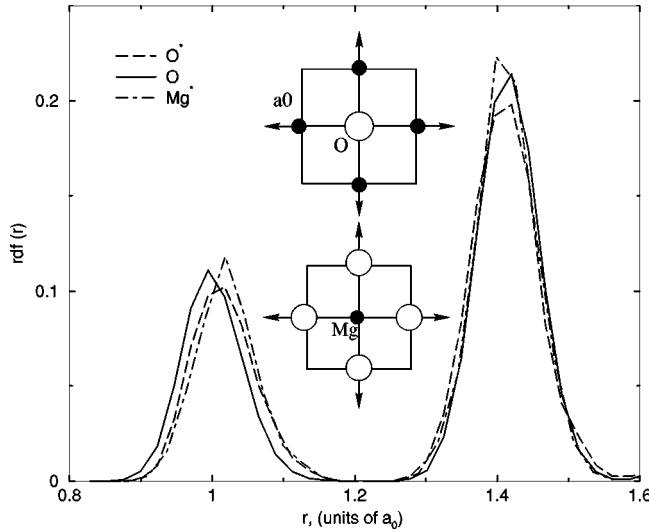


FIG. 8. The radial distribution function for oxygen ions (solid line), for fluctuating oxygen ions whose ionic charge is less negative than $q_O^{th} = \bar{Q}_O + 1.8\sigma_O$ (dashed line), and for fluctuating magnesium ions whose ionic charge is less than $q_{Mg}^{th} = \bar{Q}_{Mg} - 1.8\sigma_{Mg}$ (dot-dashed line). All the curves result from ensemble averaging over six atomic configurations generated at $T=500$ K MD. The insets show the characteristic atomic displacements around fluctuating O and Mg ions compatible with the first peak of the partial RDF's, as defined in text.

quantify this correlation, we compare the calculated probabilities for the aggregates of the fluctuating sites with those predicted by a random distribution model with the same fluctuation concentration $c(\alpha^q)$.

Assuming no correlation between fluctuations (random distribution), the probability \tilde{p}_0 for a fluctuation to have no

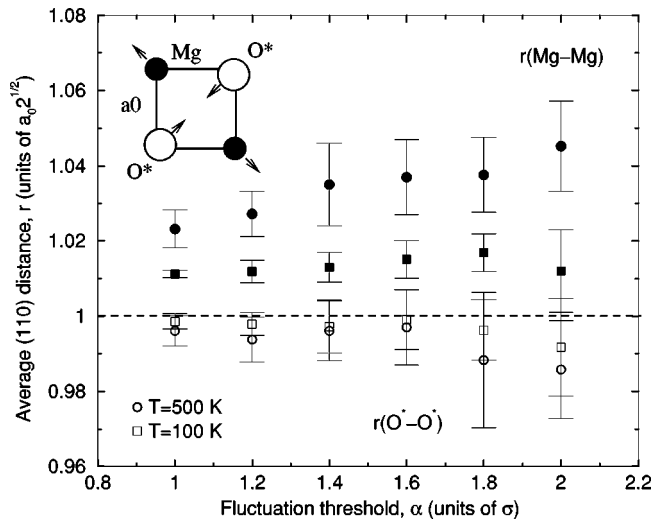


FIG. 9. The average distance in the fluctuating (110) O^*-O^* pair (open symbols) and the average distance for the (110) Mg-Mg pair adjacent to it (filled symbols) as a function of the charge fluctuation threshold α , as defined in Eq. (9). Squares correspond to an averaging over the atomic configurations at $T=100$ K, and circles to an averaging at $T=500$ K. The inset qualitatively shows the corresponding local atomic displacements.

other fluctuations on its z neighboring sites is equal to $c(1-c)^z$. Thus, \tilde{p}_0 is the probability for the isolated fluctuation. More generally, the probability to find exactly i fluctuating atoms around a chosen fluctuation is given by the expression

$$\tilde{p}_i = \binom{z}{i} c^{i+1} (1-c)^{z-i}, \quad (10)$$

where z is the coordination number in the sublattice, and $\binom{z}{i} = z! / (z-i)! i!$ is a binomial coefficient accounting for a number of possibilities for i atoms to be distributed among z sites ($z=12$ for the Mg-Mg or O-O fluctuating pairs in a rock-salt-type lattice). Thus the probability \tilde{p}_1 corresponds to a (110) fluctuating pair of ions. We find that the probabilities \tilde{p}_1 followed from the random distribution approximation [Eq. (10)] are approximately 3–4 times smaller than these obtained from an atomistic analysis. Conversely, the probabilities for the isolated fluctuations \tilde{p}_0 , predicted by the random distribution, are found to be systematically larger, thus suggesting a correlation between fluctuating sites in thermally distorted crystal. These results hold qualitatively for any value chosen for the threshold parameter α^q [Eq. (9)]. At the same time, the probabilities to find aggregates of more than two fluctuations ($i \geq 2$) depend strongly on the choice of α^q , and all vanish for the values of $\alpha^q > 2.5$.

In order to establish whether (110) pairs of charge fluctuations are coupled to the specific displacements of the nearest-neighbor atoms, it is instructive again to apply the *oscillating-well* model. For this purpose, for each fluctuating (110) pair of oxygen atoms, we find two common nearest magnesium atoms, and measure the distance between them. The average distance between the fluctuating (110) oxygens and adjacent magnesium atoms is shown in Fig. 9, as a function of a threshold fluctuation α^q for the temperatures 100 and 500 K. It is seen that the average distance between the fluctuating oxygen atoms is marginally smaller than the crystal average interatomic distance $a_0\sqrt{2}$. It depends only weakly on temperature and on α^q —the result already seen in the second RDF peak (Fig. 8). At the same time, the average distance between the adjacent Mg atoms is larger by 2–4% than $a_0\sqrt{2}$, and it correlates with both α^q and temperature. This implies that, similarly to isolated fluctuations, the fluctuations in pairs of oxygen atoms are correlated with outward displacements of the adjacent magnesium atoms, as shown in Fig. 9.

Another feature of the *relevant* potential and charge fluctuations is that they are unlikely to occur on nearest-neighbor O-Mg pair. This is seen, for example, in the significant positivity of the charge correlation function $\gamma_{OMg}(001)$ (Table I). Thus magnesium atoms, inducing the *relevant* fluctuation on the pair of oxygens, generally do not experience the *relevant* fluctuations themselves.

To summarize this section, we conclude that the potential and charge fluctuations on the oxygen atoms contributing most to the VB tail are associated with the outward breathing displacements of the nearest-neighbor magnesium atoms. They include mostly the one- and two-center fluctuations shown in Figs. 8 and 9. The fluctuating anions are effectively more positive with respect to the mean anion charge (Fig. 4).

TABLE II. Ionic charge fluctuations (i.e., deviations from the sublattice average) in the ground and excited states for six sets of atomic configurations at $T=500$ K. $S=0$ indicates the ground (singlet) state, and $S=1$ a lowest excited (triplet) state. The last column shows the triplet-singlet energy difference ΔE^{SCF} . The ΔE_0^{SCF} value corresponding to a perfect crystal is shown at the top for a comparison.

Configuration	δq_O (e)		δq_{Mg} (e)		ΔE^{SCF} (eV)
	$s=0$	$s=1$	$s=0$	$s=1$	
					10.49
1	0.04	0.70	-0.02	-0.87	5.79
2	0.02	0.77	-0.00	-0.87	6.09
3	0.01	0.72	-0.02	-0.86	6.98
4	0.02	0.69	-0.02	-0.85	7.07
5	0.02	0.80	-0.00	-0.87	5.88
6	0.01	0.54	-0.02	-0.86	7.61

Interestingly, the displacement modes associated with *relevant* anion fluctuations, are qualitatively similar to those of the one- and two-center hole polarons in cubic ionic insulators, such as MgO and alkali halides.⁴⁴ In the absence of external radiation these fluctuations vanish within the characteristic vibration times, and constantly reappear elsewhere in the lattice so that at any instant they are present in statistically important concentrations. However, when the electrons and holes are produced in the crystal (e.g. by cross-band irradiation), these fluctuations may form precursors for stable polaron states. In order to test this assumption, in Sec. VII we discuss electronic excitations in a thermally disordered crystal.

VII. ELECTRONIC EXCITATION AND SELF-TRAPPING

In modeling the electronic excitations we assume that the crystal, evolving dynamically in its electronic ground state, experiences a sudden (Frank-Condon) electronic excitation onto the lowest excited state. The latter comprises an electron in the conduction band and a hole in the valence band, which we model as a crystal triplet state ($S=1$) within the unrestricted HF approach. Hence there is one occupied state at the bottom of the conduction band in the majority spin, and one unoccupied state at the top of the valence band (a hole) in the minority spin. We carried out the excited state calculations for the 12 MgO configurations generated at 100 and 500 K. The results for $T=500$ K are presented in Table II, and can be summarized as follows.

(1) For all the atomic configurations a very strong one-center charge and spin localization (for both the electron and hole) is observed. More than 70% of a hole and more than 80% of an electron density in the excited state are localized on a single oxygen and magnesium atoms respectively (Table II).

(2) An electron and a hole can localize on either nearest-neighbor or more distant Mg and O atoms. No specific correlation between the electron and hole positions is found.

(3) The total-energy differences ΔE^{SCF} between excited and ground states for each atomic configuration are found to

be significantly lower than the value found for the ideal MgO lattice ($\Delta E_0^{SCF}=10.49$ eV) (Table II). The latter can also be compared with the highest occupied to lowest unoccupied molecular orbital gap in the ground state of the ideal lattice, 12.65 eV.

As noted above, all excitations in these calculations are essentially localized on particular atoms. It is seen in Table II that the atoms in question indeed experience strong *relevant* charge fluctuations in the ground state, that is, a positive charge fluctuation on the anion and a negative fluctuation on the cation. Furthermore, these fluctuations are substantially larger than the root-mean-square deviations of respective charge probability distributions (Fig. 7). However, the sites on which the electrons and holes are localized are not necessarily the ones on which the *relevant* fluctuations are the largest. This is due to the electron-hole Coulomb attraction, which counterbalances the repulsion tendencies of the *relevant* “holelike” and “electronlike” fluctuations [see Table I, and the discussion on the positivity of the charge correlation function $\gamma_{OMg}(100)$]. Thus the localized electron and hole may appear in either neighboring or remote sites depending on the interplay between the electron-hole Coulomb attraction and the amplitudes of the *relevant* fluctuations.

The data presented in Table II demonstrate an instant polaron localization due to the electron polarization of the lattice around fluctuating sites after an initial trapping of the electron and the hole. However, as mentioned in Sec. I, self-trapping requires that the slower lattice polarization favor the electron or hole localization (as in Fig. 1). In other words, for self-trapping to be completed, the lattice after the excitation must evolve so as to further localize the carriers. Although we have not investigated ionic dynamics in the excited state, some information can be gathered by an analysis of the forces acting on the atoms upon the excitation. We have examined the components of the Hellmann-Feynman forces along the atomic displacements of Mg ions around the pre-localized hole shown in Fig. 8. For all configurations considered at 100 and 500 K, we observe a clear tendency for the force inversion in the excited state,⁴⁵ which favors a further localization of the hole. The components of forces on the Mg ions surrounding the hole in the excited state are directed along the arrows, while those in the crystal ground state are directed against the arrows shown in Fig. 8. The situation is different for the forces on oxygen ions surrounding the localized electron. In this case we did not observe an inversion of the forces in most of the cases. This suggests that, despite the strong initial localization, the localized electron states are metastable, and dissolve quickly due to the destructive lattice relaxation. This is in agreement with the absence of intrinsic self-trapped electron states in MgO. However, the intrinsic localization of holes in pure MgO has not been observed either.

The predictions discussed here must be treated with caution, since the extent of the one-center localization in a triplet state, predicted by HF calculations, may be exaggerated. First, by virtue of parametrization, the INDO HF method does not account for the increase of the kinetic energy of the electron state due to its localization. Second, the neglect of the electron correlation within the Hartree-Fock approach is

also known to result generally in a bias toward more localized states. An optimal method for studying critical fluctuations for polaron localization would have to reproduce the extended and localized states on the same footing, and to account for electron correlation.

In search for such a method, we have carried out plane-wave density functional calculations. Thermally disordered configurations have been generated in a smaller system of 216 atoms ($3 \times 3 \times 3$ extension of the crystalline unit cell) by the shell model MD ($T=200$ K) similar to that outlined in Sec. II.

The spin-polarized DFT calculations were carried out at the generalized gradient approximation (GGA) level using the Perdew-Wang'91 functional⁴⁶ and the ultrasoft pseudopotentials⁴⁷ as supplied by Kresse and Hafner,⁴⁸ and implemented in the VASP code.⁴⁹ A charge density was calculated in the Γ point only, with an energy cutoff of 396 eV. The self-consistent excited states were modeled by constraining the total spin of the system to $S=1$ (triplet state), thus obtaining the lowest-energy state of a given multiplicity. To evaluate ionic charge and spin fluctuations, we performed a post-calculation analysis involving an integration over atomic spheres of the differential charge density between the crystal ground and triplet excited states, $[\rho_{dif}(\mathbf{r}) = \rho_{S=1}(\mathbf{r}) - \rho_{S=0}(\mathbf{r})]$, and the spin density in the excited state. The radii for the atomic spheres for the oxygen and magnesium atoms were chosen to be $R_O = a_0/\sqrt{2}$ and $R_{Mg} = a_0 - R_O$, respectively.

In contrast to the HF INDO results, the DFT calculations did not predict predominant charge or spin localization on a single lattice site. A maximum amount of a hole localized within the single oxygen sphere did not exceed 3%, (the INDO HF calculation for the same geometry predicted 83% of the hole to be localized on a single oxygen atom, and 79% of the electron to be localized on the single magnesium atom). Furthermore, $\approx 50\%$ of the exciton's electron component was found to be contained within the oxygen spheres, and only $\approx 1\%$ within the Mg spheres; the rest is spread over the interstitial regions but closer to oxygen atoms. As a result, no force inversion around the partially localized holes upon the electronic excitation was predicted by the DFT approach.

VIII. DISCUSSION

In this paper we have studied the effects of thermal disorder on the electronic properties of MgO in relation to exciton and hole polaron self-trapping and initial stages of self-trapping dynamics. To define the fingerprints of fluctuations, we have undertaken the molecular dynamics of the MgO crystal and the electronic structure for selected configurations. By means of the energy-dependent correlation functions introduced in Eqs. (3)-(5), we have established a strong correlation between the states in the band tails, fluctuations of the on-site electrostatic potential, and fluctuations of the effective ionic charge. For detecting precursor states for electron and hole trapping, we have analyzed the spatial correlations between ionic charge fluctuations coupled to the electron states deep in the DOS tails. Our main result concerns

the prediction that these fluctuations have a structural pattern statistically similar to the one- and two-center small hole polarons characteristic of dielectrics with the a rock-salt structure.^{6,17} Although the structure of the self-trapped species in these systems is well understood, it is largely unknown, whether, e.g., the stable two-center state of the hole polaron in the alkali halides evolves from one-center or multicenter initial transient states. Our results suggest that, although both one- and two-center-type atomic fluctuations are present in the ground-state MgO, only one-center holes occur in the self-consistent excited states (see Table II). It is interesting to note that similar calculations carried out for NaCl revealed that the hole component of the exciton initially localizes on either one or two anion sites, while the electron component always resides on a single cation site. These results can be used to model the evolution of the transient optical absorption of the crystals irradiated by femtosecond pulses.

The hypothesis that the configuration of the self-trapped excitons is inherited from the specific atomic fluctuations in the electronic ground state, serving as the nucleation states, can be applied to the ionic systems, where the atomic structure of the self-trapped states is not apparent. The candidate structures can be guessed upon the analysis of the correlations between the relevant potential or charge fluctuations. Some general features of these correlations, as well as of the shape of the probability distributions, can be obtained even within the classical MD approach. In particular, we have demonstrated the relation of the Gaussian character of the electrostatic potential distributions to the *oscillating-well* behavior. This finding is relevant in two respects. First, it validates for certain disordered systems a widely used Gaussian approximation for a potential distribution (see for example, Refs. 41, 50, and 51), which also follows from linear mean-field theories for polar liquids.²³ Second, it indicates where this approximation may fail. In particular, in crystals that possess no inversion symmetry, the *oscillating-well* behavior may no longer dominate, and the resulting potential distribution can become significantly non-Gaussian. This effect has been recently observed in molten salts doped with refractory metals.²¹

The next issue concerns the strong electron-lattice coupling. This manifests itself through a high sensitivity of the width of the potential probability distribution to a degree of atomic disorder (temperature). As a result, the extent of the electron band tails and the localization of the states is also strongly coupled to temperature. Therefore, under photoexcitation near the optical-absorption edge, most of the localized species may originate from fast trapping by lattice fluctuations, rather than by the much slower thermalization of band excitons. That is, excitations arrive directly in the state A_1 , as indicated in Fig. 1. This may have some implications in the photoexcitation experiments. First, providing that the further decay of self-trapped excitons leads to the formation of Frenkel defects, it may become possible to control the defects production yield by subgap irradiation. This possibility was recently reported by Lushchik *et al.* in alkali halide crystals.⁵² Second, the higher degree of atomic disorder leads to stronger fluctuations, and thus to a stronger initial local-

ization of the excitations. This would result in both the decrease of the localization time and increase of the production yield of the self-trapped excitons and their by-products with temperature. These effects should be observable at low temperatures if alternative mechanisms of the self-trapping and decay are suppressed.

A strong electron-lattice interaction also has some methodological implications for a realistic modeling of disorder at finite temperatures. As demonstrated in this paper, different Hamiltonians generate significantly different distributions of the on-site potential even when the averaging is made over the same ensembles of atomic configurations. Related to this is the issue of applicability of classical dynamics. In particular, magnesium oxide is characterized by a high Debye temperature of 941 K.^{53,54} Therefore, the effect of zero-point phonons on the atomic mean-square displacements is significant even at room temperature. Our calculation within the harmonic approximation predicts a zero-point phonon disorder amounting to 20% of the MSD for oxygen atoms at $T = 500$ K, and over 60% at $T = 100$ K. Thus classical dynamics predicts only a lower bound for characteristic ionic displacements in MgO and, hence, for the amplitudes of the characteristic potential fluctuations, electron band tails and other related properties.

Finally we should note that this work has also highlighted some of the problems characteristic of the application of many-electron theory to the polaron phenomena. Two (possibly interrelated) aspects are important here: the origin of the conduction band and the exciton localization properties. Our electron localization analysis in DFT calculations, although somewhat dependent on an arbitrary choice of ionic spheres, highlights a general controversy in the present understanding of the nature of the conduction band in MgO and other cubic oxides. Providing that, in the crystal triplet state, the electron occupies a state at the bottom of the CB, spin-polarized DFT calculations imply that the latter is predominantly determined by the oxygen $3s$ atomic orbitals. This is in agreement with the recent local-density-approximation (LDA)-based band structure analysis presented by de Boer and de Groot.⁵⁵ However, band-structure calculations based on non-DFT techniques⁵⁶ predicted the CB in MgO to be predominantly of magnesium $3s$ character (also see the discussion by Kantorovich *et al.*⁵⁷).

One of the reasons for this discrepancy is an uncorrected self-interaction in the LDA and GGA density functionals. The problem becomes more apparent in calculations of a triplet exciton. Here the local exchange approximation may significantly underestimate the repulsion of the electrons with the same spin, resulting in both of them being localized on the same sublattice. The exact account of the exchange interaction will result in spin separation, and, hence, will enhance the magnesium participation in the states occupied by the electron. At the same time, self-interaction results in a bias toward a more delocalized charge density, as reported in a number of studies (see, for example, Refs. 25 and 29–32). A systematic study of the effect of self-interaction on localization is hindered by the lack of tractable methods going beyond the GGA approximation, as well as by many other factors affecting the localization properties in practical calculations, such as incomplete basis sets, the pseudopotential approximation, lattice polarization effects, and spurious electrostatic interactions across the periodically repeated supercells. An extensive study is required to separate these influences, which is currently underway.

We note in conclusion that both the HF INDO and plane-wave DFT methods used in this study do not predict a correct balance between different contributions to the polaron self-trapping energy, the former overestimating and the latter underestimating the degree of initial localization of the excited carriers. Thus, in order to discriminate between the localized and extended electronic states more refined methods are required.

ACKNOWLEDGMENTS

The authors gratefully acknowledge funding by the Leverhulme Trust and NATO Grant No. CRG.974075. DFT and MD calculations were performed on the CRAY T3E supercomputer facility provided by the Materials Chemistry Consortium, UK, and on the Bentham computer at the HiPerSpace Center at the University College London. The authors are grateful to A. M. Stoneham, R. T. Williams, A. A. Sokol, A. H. Harker, and D. Bowler for many stimulating discussions and for their comments on the manuscript.

*Email address: j.gavartin@ucl.ac.uk

¹K. S. Song and R. T. Williams, *Self-Trapped Excitons*, 2nd ed. (Springer, New York, 1996).

²E. I. Rashba, in *Excitons*, edited by E. I. Rashba and M. D. Sturge (North-Holland, Amsterdam, 1982), p. 544.

³Y. Toyozawa, *J. Lumin.* **24-25**, 23 (1981).

⁴H. Sumi and Y. Toyozawa, *J. Phys. Soc. Jpn.* **31**, 342 (1971).

⁵H. Sumi and A. Sumi, *Phys. Soc. Jpn.* **56**, 2211 (1987).

⁶A. L. Shluger and A. M. Stoneham, *J. Phys.: Condens. Matter* **5**, 3049 (1993).

⁷S. Guizard, P. Martin, Ph. Daguzan, G. Petite, P. Audebert, G. P. Geindre, A. Dos Santos, and A. Antonetti, *Europhys. Lett.* **29**, 401 (1995).

⁸P. Martin, S. Guizard, Ph. Daguzan, G. Petite, P. D'Oliveira, P.

Meynadier, and M. Perdrix, *Phys. Rev. B* **55**, 5799 (1997).

⁹S. Iwai, T. Tokizaki, A. Nakamura, T. Shibata, A. L. Shluger, and N. Itoh, *J. Lumin.* **60**, 720 (1994).

¹⁰S. Iwai, T. Tokizaki, A. Nakamura, K. Tanimura, N. Itoh, and A. Shluger, *Phys. Rev. Lett.* **76**, 1691 (1996).

¹¹H. Fujiwara, T. Suzuki, and K. Tanimura, *Mater. Sci. Forum* **239-241**, 561 (1997).

¹²K. Tanimura and H. Fujiwara, *Mater. Sci. Forum* **239-241**, 549 (1997).

¹³L. Landau, *Phys. Z. Sowjetunion* **3**, 664 (1933).

¹⁴E. N. Economou and C. M. Soukoulis, *Phys. Rev. B* **28**, 1093 (1983); E. N. Economou, C. M. Soukoulis, and A. D. Zdetsis, *ibid.* **30**, 1686 (1984).

¹⁵C. M. Soukoulis and E. N. Economou, *Waves Random Media* **9**,

- 255 (1999).
- ¹⁶D. Emin and M.-N. Bussac, Phys. Rev. B **49**, 14 290 (1994).
- ¹⁷A. L. Shluger and J. D. Gale, Phys. Rev. B **54**, 962 (1996).
- ¹⁸E. D. Thoma, H. M. Yochum, and R. T. Williams, Phys. Rev. B **56**, 8001 (1997).
- ¹⁹P. K. Schelling and J. W. Halley, Phys. Rev. B **62**, 3241 (2000).
- ²⁰T. Koslowski, Ber. Bunsenges. Phys. Chem. **100**, 95 (1996).
- ²¹T. Koslowski, J. Chem. Phys. **113**, 10 703 (2000).
- ²²T. Koslowski and D. E. Logan, J. Phys. Chem. **98**, 9146 (1994).
- ²³D. E. Logan and F. Siringo, J. Phys.: Condens. Matter **4**, 3695 (1992).
- ²⁴A. L. Shluger, J. L. Gavartin, M. A. Szymanski, and A. M. Stoneham, Nucl. Instrum. Methods Phys. Res. B **166-167**, 1 (2000).
- ²⁵J. L. Gavartin and A. L. Shluger, Radiat. Effects Defects Solids (to be published).
- ²⁶S. Knief, W. von Niessen, and T. Koslowski, Phys. Rev. B **58**, 4459 (1998).
- ²⁷S. J. Sarnthein, A. Pasquarello, and R. Car, Phys. Rev. Lett. **74**, 4682 (1995).
- ²⁸T. Koslowski, W. Kob, and K. Vollmayr, Phys. Rev. B **56**, 9469 (1997).
- ²⁹R. Dovesi, R. Orlando, C. Roetti, C. Pisani, and V. R. Saunders, Phys. Status Solidi B **217**, 63 (2000).
- ³⁰G. Pacchioni, F. Frigoli, D. Ricci, and J. A. Weil, Phys. Rev. B **63**, 054102 (2001).
- ³¹J. Laegsgaard and K. Stokbro, Phys. Rev. Lett. **86**, 2834 (2001).
- ³²V. Perebeinos, P. B. Allen, and M. Weinert, Phys. Rev. B **62**, 12 589 (2000).
- ³³W. Cochran, CRC Crit. Rev. Solid State Mater. Sci. **2**, 1 (1971).
- ³⁴D. Fincham, W. C. Mackrodt, and P. J. Mitchell, J. Phys.: Condens. Matter **6**, 393 (1994).
- ³⁵M. Gillan and P. Lindan, J. Phys.: Condens. Matter **5**, 1019 (1993).
- ³⁶J. D. Gale, J. Chem. Soc., Faraday Trans. **93**, 69 (1997).
- ³⁷A. M. Stoneham and M. J. L. Sangster, Philos. Mag. B **52**, 717 (1985).
- ³⁸W. H. Press, S. A. Teukolsky, W. T. Vetterling, and B. P. Flannery, *Numerical Recipes in Fortran. The Art of Scientific Computing*, 2nd ed. (Cambridge University Press, Cambridge, 1992).
- ³⁹L. N. Kantorovich, A. Stashans, E. A. Kotomin, and P. W. M. Jacobs, Int. J. Quantum Chem. **52**, 1177 (1994).
- ⁴⁰E. V. Stefanovich, E. K. Shidlovskaya, A. L. Shluger, and M. A. Zakharov, Phys. Status Solidi B **160**, 529 (1990).
- ⁴¹J. Ziman, *Models of Disorder: The Theoretical Physics of Homogeneously Disordered Systems* (Cambridge University Press, Cambridge, 1971).
- ⁴²J. Pople and D. Beveridge, *Approximate Molecular Orbital Theories* (McGraw-Hill, New York, 1970).
- ⁴³J. Ziman, *Principles of the Theory of Solids* (Cambridge University Press, Cambridge, 1965).
- ⁴⁴A. M. Stoneham, *Theory of Defects in Solids* (Clarendon Press, Oxford, 1975), p. 653.
- ⁴⁵On rare occasions we found that in the ground state the force components on some atoms were directed away from the fluctuating atom, but the magnitude of these forces would be very small. In the excited state these forces would keep their direction and increase in magnitude.
- ⁴⁶J. P. Perdew and Y. Wang, Phys. Rev. B **46**, 12 947 (1992).
- ⁴⁷D. Vanderbilt, Phys. Rev. B **41**, 7892 (1990).
- ⁴⁸G. Kresse and J. Hafner, J. Phys.: Condens. Matter **6**, 8245 (1994).
- ⁴⁹G. Kresse and J. Hafner, Phys. Rev. B **47**, R558 (1993); G. Kresse and J. Furthmuller, *ibid.* **54**, 11 169 (1996).
- ⁵⁰P. A. Lee and T. V. Ramakrishnan, Rev. Mod. Phys. **57**, 287 (1985).
- ⁵¹T. -M. Chang, J. D. Bauer, and J. L. Skinner, J. Chem. Phys. **93**, 8973 (1990).
- ⁵²A. Lushchik, M. Kirm, Ch. Lushchik, and E. Vasil'chenko, Nucl. Instrum. Methods Phys. Res. B **166-167**, 529 (2000).
- ⁵³T. H. K. Barron, W. T. Berg, and J. A. Morrison, Proc. R. Soc. London, Ser. A **250**, 70 (1959).
- ⁵⁴Our shell model predicts the Debye temperature for MgO to be $\theta_D=1050$ K (neglecting the effects of thermal volume expansion). An account of the lattice thermal expansion in the calculation would lower θ_D , in closer agreement with experiment.
- ⁵⁵P. K. de Boer and R. A. de Groot, J. Phys.: Condens. Matter **10**, 10 241 (1998).
- ⁵⁶W. Y. Ching, F. Gan, and M.-Z. Huang, Phys. Rev. B **52**, 1596 (1995); R. Pandey, J. E. Jaffe, and A. B. Kunz, *ibid.* **43**, 9228 (1991).
- ⁵⁷L. N. Kantorovich, J. M. Holender, and M. J. Gillan, Surf. Sci. **343**, 221 (1995).